Spatial and temporal interference during the ionization of H by few-cycle XUV laser pulses

S. Borbély,[1,*] A. Tóth,[1] K. Tőkési,[2] and L. Nagy[1]

[1]*Faculty of Physics, Babeş-Bolyai University, Kogălniceanu Street No. 1, 400084 Cluj, Romania*

[2]*Institute of Nuclear Research of the Hungarian Academy of Sciences (ATOMKI), P. O. Box 51, H-4001 Debrecen, Hungary*

(Received 29 August 2012; published 4 January 2013)

We have investigated the ionization of H atoms by few-cycle XUV laser pulses, in particular the interference between electronic wave packets emitted at different time moments (temporal interference), and the interference between wave packets emitted at the same time, but following different paths (spatial interference). During the spatial interference, under appropriate conditions, the holographic mapping (HM) of the target atom's state is achieved, which has the potential to become a powerful tool to study atomic structure. First, by using classical trajectory Monte Carlo calculations, we have confirmed the existence of two distinct types of electron trajectories, which contribute to the formation of the HM interference pattern. Then, by using *ab initio* quantum-mechanical calculations, we have studied how the shape of the HM pattern is influenced by the laser pulse parameters. Finally, we have identified the optimal laser pulse parameters for the observation of the HM interference in the case of atomic species with an ionization potential close to 0.5 a.u.

DOI: 10.1103/PhysRevA.87.013405 PACS number(s): 32.80.Fb, 33.60.+q, 61.05.jp, 31.15.A−

I. INTRODUCTION

With the recent development of laser technology, few-cycle laser pulses are routinely produced for a wide range of photon frequencies [1]. At high field intensities, when such a laser pulse interacts with atomic systems, the dominant process is the ionization (above-threshold, tunneling, or over-the-barrier ionization, depending on the Keldysh parameter [2]). During and after the ionization, secondary processes also occur, which have a significant impact on the final momentum distribution of the electrons. As discussed in detail by Bian *et al.* [3], these are the result of interference between electronic wave packets following different paths. From the numerous possible scenarios [3], only two have a significant impact (measurable in experiments) on the final momentum distribution of the free electrons.

In the first scenario, electronic wave packets emitted at different parts of the laser pulse (i.e., at different time moments) interfere, leading to a fringe structure in the electron energy spectrum [4], consisting of circular interference maxima and minima, which are perpendicular to the laser polarization [4,5]. This process can be interpreted as a double- (multi-) slit interference in time domain [4], and it was studied in detail by several groups both theoretically [3,5–7] and experimentally [4,8]. The structure of this interference pattern can be understood and described accurately in a simple semiclassical picture [3–5], where the electronic wave packets with the same asymptotic momentum are emitted at different time moments. These wave packets follow different paths under the combined action of the external laser field and of the core's Coulomb potential accumulating different final phases. In the continuum, when they are coherently added, they amplify or cancel each other out, depending on their relative phase, leading to a measurable [4,8] fringe pattern in the electron spectrum.

In the second scenario, electronic wave packets emitted at the same time (i.e., during the same quarter-pulse cycle) follow different paths, accumulating different final phases, leading to a radial fringe structure in the electron spectra [3,5,9,10]. In a simplistic picture [3,9,10], the radial fringe structure is a result of the interference between the direct (i.e., unscattered) and the scattered wave packets, where the direct wave packet can be considered as a reference while the scattered wave packet as a signal wave. In this picture, the interference fringe structure can be interpreted as the holographic mapping (HM) of the target atom's or molecule's state [10]. This holographic imaging is strongly related to the laser-induced electron diffraction (LIED) [11–15], where the electron wave packets induced by the ultrashort laser pulse are used to map the structure of the parent ion via electron wave packet diffraction. From the final electron momentum distribution resulting from LIED, both structural [11–14] and temporal [15] information regarding the target atom or molecule can be extracted using laborious procedures [13]. In contrast to LIED, in the HM, in addition to the diffracted (scattered) electron wave packet a reference wave packet is also present, and the interference between these two leads to a more structured electron momentum distribution with interference minima and maxima. Since the location of these interference extrema is strongly influenced by the short-range potential encoding the structure of the target atom or molecule, the HM is a potentially powerful tool to investigate the internal structure of atoms and molecules.

All previous studies [3,9,10] investigated the HM interference effects only in the near-IR and IR photon energy region (i.e., for ω photon energies smaller than 0.12 a.u.), and in the many-cycle regime. These studies were mainly focusing on finding the laser pulse parameters for which the HM pattern appears without investigating in detail how the shape of the HM pattern is influenced by these parameters. Due to the small photon energy and the many field cycles used in the previous studies, the measured and calculated photoelectron momentum distributions were narrow, mainly concentrated around the Oz polarization axis of the laser field, which allowed only the observation of a few interference extrema. For a detailed study on the shape of the HM pattern as a function of laser field parameters (important for its application as a

*sandor.borbely@phys.ubbcluj.ro;http://sandorborbely.ro

tool to investigate atomic and molecular structures), a much broader continuum electron distribution is needed. This can be achieved by increasing the photon energy, and by considering only few-cycle laser pulses. The use of few-cycle pulses, beside ensuring a wide photoelectron momentum distribution, also gives us the opportunity to control the electronic dynamics through the carrier-envelope phase parameter, ϕ_0. By choosing the proper value for ϕ_0, we have ensured that in the ionization spectra, the HM pattern became the dominant feature, which was not achievable with laser pulses used in the previous studies.

Based on these motivations, in this work we theoretically investigate the conditions under which the HM appears for higher photon energies (0.2 a.u. $< \omega <$ 0.7 a.u.) during the ionization of H by few-cycle laser pulses using classical and quantum-mechanical models. The main goal of our study is to probe how the shape of the HM interference fringes depends on the laser field parameters, and to identify the relevant field parameters determining their shape. A detailed understanding of the HM for the H atom (i.e., for a simple Coulomb scattering field) is crucial for future applications, since structural information can be extracted from the HM of more complex targets by comparing them with the hydrogenic HM.

The article is structured as follows. In Sec. II, we summarize the theoretical methods used in the present studies, namely the direct solution of the time-dependent Schrödinger equation using the time-dependent close-coupling method (TDCC model), the classical trajectory Monte Carlo method (CTMC model), and the simple two-path model [10] for the HM. In Sec. III, the obtained results are presented and discussed. Snapshots on a typical time evolution of the studied H atom found in an external few-cycle XUV laser field are presented discussing the dominant processes as they appear. This is followed by a study on how the HM interference pattern is influenced by the laser pulse parameters (i.e., by photon energy and field intensity). In the last section, final conclusions are drawn and an outlook on the possible continuation of the present work is presented.

Throughout the present article, atomic units are used.

II. THEORETICAL METHODS

In this section, the studied system, i.e., the hydrogen atom in an external electromagnetic field, is presented along with the classical and quantum-mechanical models used to describe its time evolution. The Hamiltonian of this system is

$$\hat{H} = \frac{\hat{p}^2}{2m} + V(\vec{r}) + \vec{r}\cdot\vec{E}(t), \tag{1}$$

where $\hat{p}^2/2m$ is the kinetic energy operator of the electron, $V(\vec{r}) = -1/r$ is the Coulomb potential, and $\vec{r}\cdot\vec{E}(t)$ is the interaction between the electron and the external laser field expressed in length gauge in the framework of the dipole approximation. Here the external laser field is characterized by its electric component using a simple plane wave modulated by a sine-square envelope function as follows:

$$\vec{E}(t) = \begin{cases} \hat{\varepsilon} E_0 \sin^2\left(\frac{\pi t}{\tau}\right)\sin(\omega t + \phi_0) & \text{if } t \in (0,\tau), \\ 0 & \text{elsewhere,} \end{cases}$$

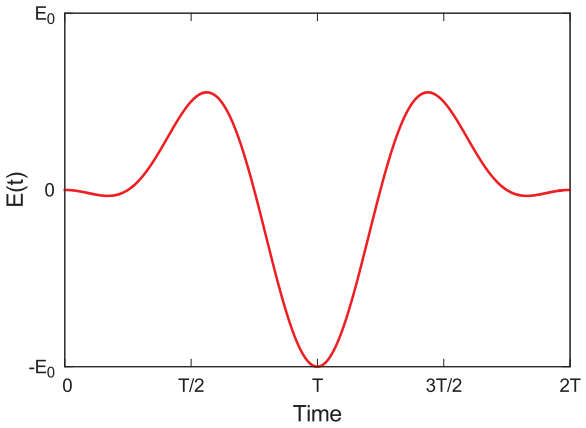

FIG. 1. (Color online) The shape of the two-cycle, cosinelike laser pulses used in our calculations, where $T = 2\pi/\omega$ is the period of the carrier wave.

where $\hat{\varepsilon}$ is the polarization of the laser field, ω is the frequency of the carrier wave, ϕ_0 is the carrier-envelope phase, and τ is the pulse duration.

As discussed in [5], the ϕ_0 carrier-envelope phase is the critical parameter, which, through the shape of the few-cycle laser pulse, determines which secondary process is dominant: for a sinelike pulse, the intercycle interference is dominant, while for a cosinelike pulse, the HM is dominant. Since the main goal of the present work is to study the HM, cosinelike two-cycle laser pulses (see Fig. 1) were used during the calculations, for which the carrier-envelope phase is

$$\phi_0 = -\frac{\omega\tau}{2} - \frac{\pi}{2}.$$

A. The TDCC model

The time evolution of the hydrogen atom driven by the above-presented two-cycle laser pulses is described by the time-dependent Schrödinger equation

$$i\frac{\partial}{\partial t}\Psi(\vec{r},t) = \hat{H}\Psi(\vec{r},t), \tag{2}$$

where $\Psi(\vec{r},t)$ is the electronic time-dependent wave function. Since the exact analytic solution of the Schrödinger equation (2) is not known, in the present work its direct numerical solution is performed using the well established time-dependent close-coupling method [16]. In the TDCC approach, the time-dependent wave function is expanded into terms of spherical harmonics,

$$\Psi(\vec{r},t) = \sum_{lm}\frac{R_{lm}(r,t)}{r}Y_{lm}(\Omega_r). \tag{3}$$

By substituting the expansion (3) into the Schrödinger equation for the $R_{lm}(r,t)$ radial wave functions, the following set of coupled partial differential equations (PDEs) is obtained:

$$i\frac{\partial}{\partial t}R_{lm}(r,t) = \sum_{l'm'}\left(T_{lml'm'} + V^{\mathrm{CP}}_{lml'm'} + V^{\mathrm{C}}_{lml'm'} + V^{\mathrm{EL}}_{lml'm'}\right)R_{l'm'}(\vec{r},t), \tag{4}$$

where

$$T_{lml'm'} = -\delta_{ll'}\delta_{mm'}\frac{\partial^2}{\partial r^2}$$

is the kinetic energy matrix element,

$$V^{\mathrm{CP}}_{lml'm'} = \delta_{ll'}\delta_{mm'}\frac{l(l+1)}{r^2}$$

is the centrifugal potential energy matrix element,

$$V^{\mathrm{C}}_{lml'm'} = -\delta_{ll'}\delta_{mm'}\frac{1}{r}$$

is the Coulomb potential matrix element, and

$$V^{\mathrm{EL}}_{lml'm'} = rE(t)\sqrt{\frac{3(2l+1)}{4\pi(2l'+1)}}C^{l'm'}_{10lm}C^{l'0}_{10l0}$$

is the electron-laser interaction matrix element, with C being the Clebsch-Gordan coefficients. By using the TDCC approach, the three-dimensional (3D) Schrödinger equation is reduced to a finite set of coupled 1D PDEs, which is much easier to handle than the original problem.

For the discretization of the radial coordinates, we have used the finite-element discrete variable representation (FEDVR) method [17,18]. In the present FEDVR approach, we have divided the radial coordinate into finite elements (FEs), and inside each FE the radial wave functions $R_{lm}(r,t)$ are represented on a local discrete variable representation (DVR) basis. To ensure the continuity of the wave functions at FE boundaries, the local DVR basis was built on top of Gauss-Lobatto quadrature points.

For the temporal propagation of our system, i.e., for the solution of (4), we have used the standard fourth-order Runge-Kutta method. From the time-dependent wave functions, the momentum distribution of the free electrons was obtained by direct projection into exact continuum eigenstates of the unperturbed $\hat{H}_0 = \hat{p}^2/2m + V(\vec{r})$ atomic Hamiltonian. At the end of the laser pulse, this momentum distribution is equivalent to the ionization probability density measurable by experiments.

B. The CTMC model

In addition to the exact quantum-mechanical calculations (TDCC model), classical stochastic calculations within the framework of the classical trajectory Monte Carlo method were performed in order to get a deeper insight into the physics of the investigated processes. The CTMC method is a nonperturbative method in which classical equations of motion are solved numerically. A microcanonical ensemble characterizes the initial state of the target from which individual initial conditions of the target are taken. In the present CTMC approach, Newton's classical nonrelativistic equations of motion are solved [19–21] numerically by integrating with respect to time as an independent variable using the standard Runge-Kutta method until the real exit channels are obtained. For the ionization channel, the final energy and the scattering angles (both polar and azimuthal) of the ionized electron were recorded, from which the momentum distribution of the electrons was calculated.

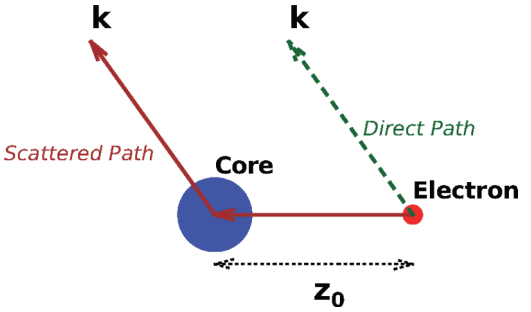

FIG. 2. (Color online) The direct and scattered electron trajectories in the two-path model.

C. Two-path model

In their recent publication [10], Huismans and co-workers presented a simple, intuitive model to grasp the essence of the HM. In this model, an electronic wave packet is formed (via tunneling or over-the-barrier ionization) at a z_0 distance from the core, which is then returned by the laser field and scattered on the core considered as a uniform point scatterer. As indicated in Fig. 2, an electron from this wave packet with final momentum $\vec{k}$ may follow two different paths: a direct or a scattered one. Within this simplified picture, the difference between the phases accumulated by the electrons on the two possible paths can be calculated analytically. Using this phase difference the pattern resulting from the interference of the two electron paths can be given as

$$I(\vec{k}) \sim |1 + e^{iz_0(k-k_z)}|, \tag{5}$$

and it is plotted for $z_0 = 5$ a.u. in Fig. 3. The beauty of this model is that the interference pattern is influenced by only one relevant parameter, z_0. With increasing z_0, the density of the interference fringes also increases.

III. RESULTS AND DISCUSSIONS

To identify the processes occurring during the interaction of few-cycle XUV pulses with the H atom, we have presented snapshots on the time evolution of such a system in Fig. 4.

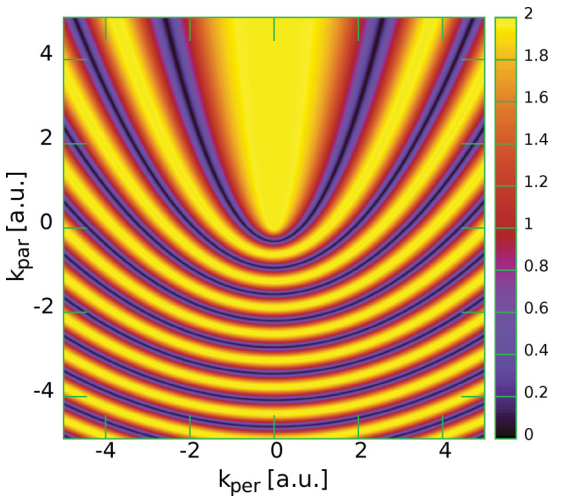

FIG. 3. (Color online) The two-path interference pattern for $z_0 = 5$ a.u.

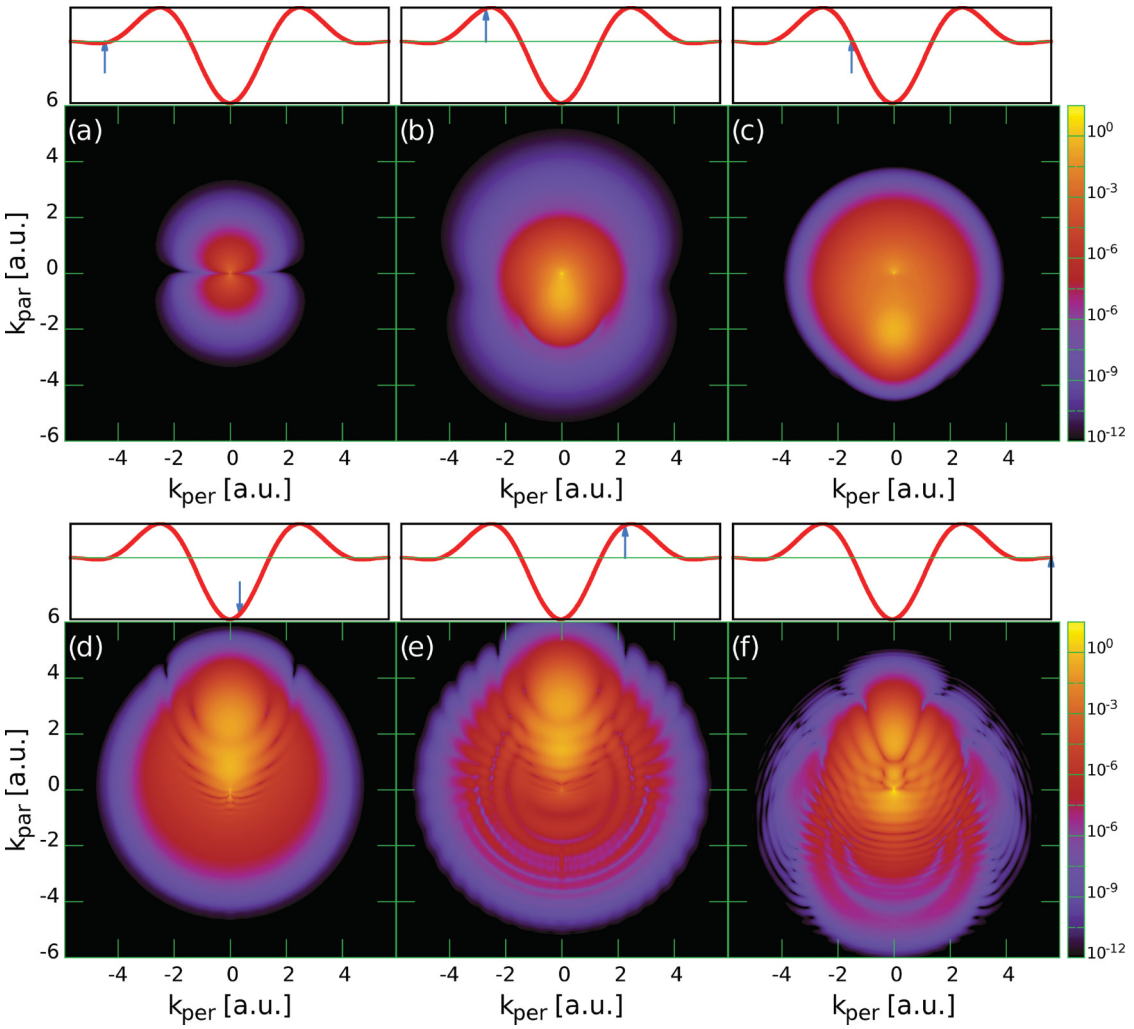

FIG. 4. (Color online) Momentum distribution of the continuum electrons as a function of parallel and perpendicular momentum components at different time moments indicated by the arrows on the laser pulse. Laser pulse parameters: $\omega = 0.4445$ a.u., $E_0 = 1$ a.u., and $\tau = 28.26$ a.u.

The parameters of the laser pulse were chosen as follows: $\omega = 0.4445$ a.u., $E_0 = 1$ a.u., and $\tau = 4\pi/\omega = 28.26$ a.u. On each snapshot the distribution of the continuum electrons is plotted as a function of momentum components parallel (k_{par}) and perpendicular (k_{per}) to the laser pulse polarization. Above each momentum distribution, the corresponding time is indicated by an arrow on the laser pulse.

At the beginning of the laser pulse ($t < 5$ a.u.), the continuum electrons show a dipolelike momentum distribution [see Fig. 4(a)] indicating single-photon ionization. However, by taking a look at Fig. 5, where the total ionization probability is plotted as a function of time, we can conclude that the overall contribution of this single-photon ionization is negligible. Progressing further in time, we observe a sudden increase in the strength of the laser field, which drives the large increase in the total ionization probability observed between $t = 5$ and 10 a.u. These photoelectrons are mainly emitted in the direction of the laser field polarization, and they exhibit a strong forward-backward asymmetry [see Fig. 4(b)], indicating that the dominant ionization process is the tunneling and the over-the-barrier ionization. This newly formed electronic wave packet is moving under the combined action of the electric fields generated by the parent ion and the laser pulse. First, under the action of the strong laser field, it leaves the vicinity of the parent ion [Fig. 4(c)], and when the direction of the laser field changes

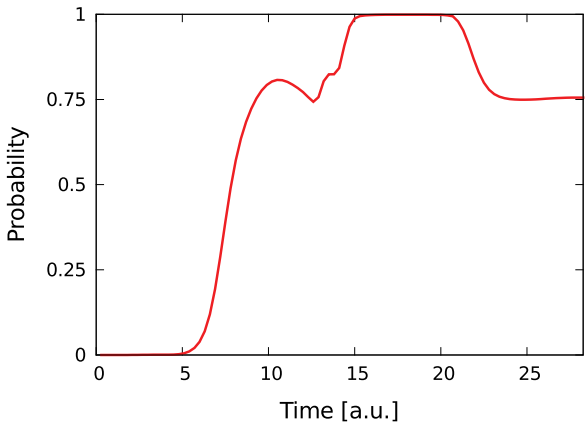

FIG. 5. (Color online) The total ionization probability as a function of time. Laser pulse parameters: $\omega = 0.4445$ a.u., $E_0 = 1$ a.u., and $\tau = 28.26$ a.u.

($t \sim 10$ a.u.), it is driven back to the core. Further on, this returning wave packet is scattered by the parent ion, leading to the HM interference pattern plotted in Fig. 4(d). This pattern is similar in structure to the one obtained in the framework of the simple two-path model shown in Fig. 2. Progressing further in time, concentric rings of maxima and minima appear in the ionization probability density [see Fig. 4(e)], which may be identified as the temporal interference pattern. This pattern is the result of the interference between electronic wave packets emitted at different time moments under the action of the laser field. At this moment, all important features of final momentum distribution [Fig. 4(f)] are formed, and only minor modifications in shape are present due to the further quiver motion of the electrons and due to the electron recapture at the end ($t > 25$ a.u.) of the laser pulse. In accordance with the conclusions of Arbó *et al.* [5], in the case of our cosine-shaped pulse, the spatial interference (the radial HM pattern) is dominant over the temporal interference (concentric circles), which is barely visible even on a logarithmic scale.

A. Temporal interference effects

As pointed out in the previous section, the concentric circles of maxima and minima in Fig. 4(f) may be explained as the result of the interference between the electronic wave packets emitted at different time moments. In addition to this qualitative explanation, a more detailed quantitative analysis can be performed using a strong field approximation (SFA) approach, where after the ionization the action of the Coulomb potential is neglected. In this picture, the first electronic wave packet is emitted at time moment t_1 with $\vec{k}_1(t_1)$ momentum, while the second electronic wave packet is emitted at time moment t_2 with $\vec{k}_2(t_2)$ momentum. To have constructive or destructive interference between these wave packets, the following equation has to be satisfied:

$$\vec{k}_1(t_2) = \vec{k}_2(t_2). \tag{6}$$

Since in the SFA the Coulomb potential is neglected, we can write that

$$\vec{k}(t_2) - \vec{k}(t_1) = -\int_{t_1}^{t_2} \vec{E}(t)dt = \vec{A}(t_2) - \vec{A}(t_1), \tag{7}$$

where

$$\vec{A}(t) = -\int_0^t \vec{E}(x)dx,$$

thus the condition (6) for the interference reads

$$\vec{k}_1(t_1) + \vec{A}(t_2) - \vec{A}(t_1) = \vec{k}_2(t_2). \tag{8}$$

The phase accumulated by the first wave packet in the time interval $[t_1,t_2]$ can be calculated as follows:

$$\Delta\phi[\vec{k}_1(t_1),t_1,t_2] = \int_{t_1}^{t_2} \frac{\vec{k}_1(t)^2}{2}dt, \tag{9}$$

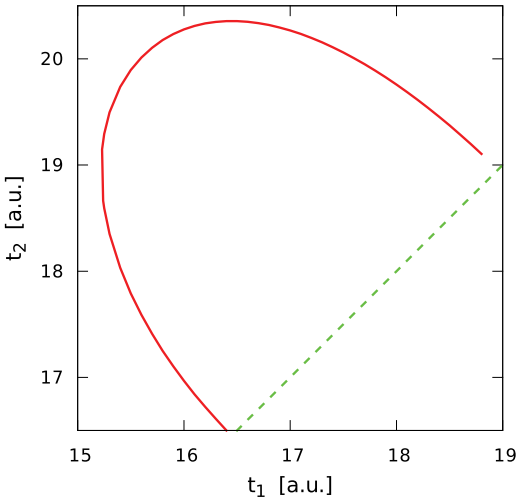

FIG. 6. (Color online) Solid line: $t_2 > t_1$ values for which the center of the interference circles is located at $k_{z_0} = -1.898$ a.u. Dashed line: $t_2 = t_1$ line.

which can be expressed as a function of the asymptotic $\vec{k}_1(t = \tau)$ electron momentum using Eq. (7):

$$\Delta\phi[\vec{k}_1(\tau),t_1,t_2] = \int_{t_1}^{t_2} \frac{[\vec{k}_1(\tau) + \vec{A}(t)]^2}{2}dt. \tag{10}$$

The pattern resulting from the temporal interference within the framework of the SFA is described by

$$I(\vec{k},t_1,t_2) \sim |1 + e^{i\Delta\phi(\vec{k},t_1,t_2)}|, \tag{11}$$

which is formed by concentric circles of interference maxima and minima. By fitting the SFA interference pattern (11) to the one obtained during the exact TDCC calculations [Fig. 4(f)], we were able to calculate the t_1 and t_2 emission times for the interfering electron wave packets as follows. First, based on the TDCC results, we have fixed the center of the interference circles at $k_{z_0} = -1.898$ a.u., which gave us a constraint for the t_1 and t_2 values shown in Fig. 6. From these $\{t_1,t_2\}$ values, we choose those for which the second SFA minimum matched with the second TDCC minimum. Applying this approach, we have found two pairs of $\{t_1,t_2\}$ values (see Fig. 7, upper part): {15.25,18.59}, {17.00,20.26}, which reproduced the TDCC interference rings. In the lower part of Fig. 7 one can observe the SFA extrema rings (indicated by white circles), which are in good agreement with TDCC calculations. The small discrepancies which are present can be explained by the fact that in the SFA approach, the influence of the Coulomb potential on the final electron momenta and on the $\Delta\phi$ phase shift is neglected. From the obtained $\{t_1,t_2\}$ pairs, in agreement with the findings of [3], we can conclude that the concentric circles observed in the momentum distribution of the continuum electrons are the result of the interference between the electronic wave packets emitted at opposite half-cycles of the same laser field cycle.

B. Spatial interference effects

As discussed at the beginning of the present section, during the return of the electronic wave packet formed via tunneling and over-the-barrier ionization, scattering on the parent ion

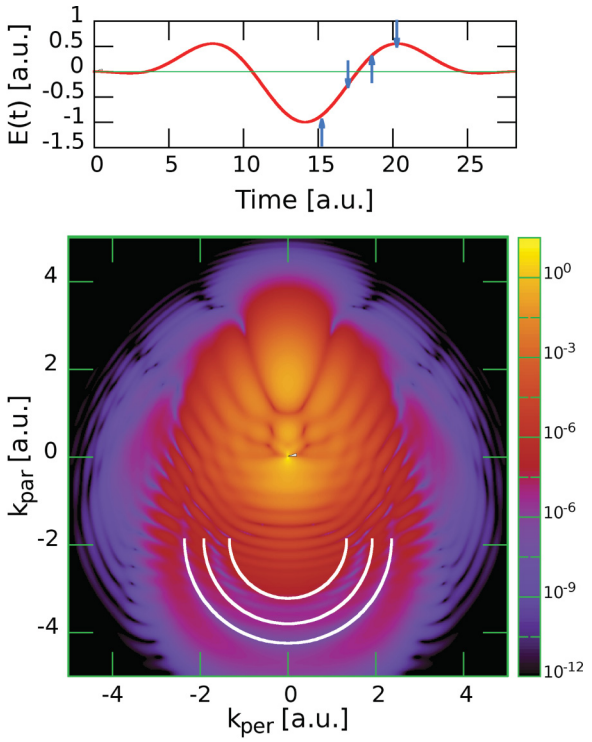

FIG. 7. (Color online) SFA interference rings (white circles) on top of the TDCC ionization probability density expressed as a function of parallel and perpendicular momentum components. Laser pulse parameters: $\omega = 0.4445$ a.u., $E_0 = 1$ a.u., and $\tau = 28.26$ a.u. On the upper figure, the "up arrows" indicate the {15.25,18.59} pairs of $\{t_1,t_2\}$ values, while the "down arrows" indicate the {17.00,20.26} pairs of $\{t_1,t_2\}$ values.

occurs. Under the right conditions, this scattering leads to the formation of a radial interference pattern [see Fig. 4(d)], which can be interpreted as the holographic mapping (HM) of the parent ion's state [3,9,10]. The formation of the HM pattern can be explained qualitatively using the simple two-path model of Huismans *et al.* [10] presented in Sec. II C. The basic assumption of the two-path model is that during the scattering, electrons may follow two different paths: one close to the core (scattered path) and one far from the core (direct path). To test the validity of this assumption, we have performed CTMC calculations. With the exception of the interference effects, a good overall agreement between the TDCC and CTMC momentum distributions can be observed (see Fig. 8). This general agreement allows us to perform detailed analysis of the CTMC electron trajectories. We further suppose that the quantum-mechanical electron dynamics is not far from the classical one. From the calculated CTMC trajectories, we have selected those which contribute to the formation of the HM pattern, namely those where the electron is ionized at the very beginning of the laser pulse and then returned to the vicinity of the parent ion by the laser field. For each of those trajectories, we have calculated the value of $r_{\min}$, which measures how close the electron drives by the core in the return phase. If all selected trajectories are considered, the obtained distribution of the $r_{\min}$ values is broad [see Fig. 9(a)] without any characteristic feature. However, if we consider only those CTMC trajectories where the asymptotic momentum is fixed

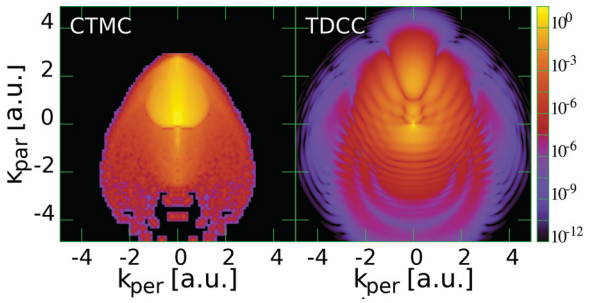

FIG. 8. (Color online) Ionization probability densities as a function of parallel and perpendicular momentum components obtained in the framework of the CTMC and TDCC models. Laser pulse parameters: $\omega = 0.4445$ a.u., $E_0 = 1$ a.u., and $\tau = 28.26$ a.u.

(these trajectories interfere with each other), the distribution of the $r_{\min}$ values completely changes. We will have two well separated groups of trajectories [see Fig. 9(b)]: those with small $r_{\min}$ considered to be scattered, and those with large $r_{\min}$ considered to be direct. These findings confirm the assumption of the two-path model, i.e., the existence of two distinct types of electron paths during the scattering.

The main prediction of the two-path model is that the density of the HM interference fringes is determined by the value of z_0, i.e., how far the formed electronic wave packet departs from the parent ion. The value of z_0 depends mainly on the value of the average value of the electronic wave packet's velocity, and on how much time the wave packet has to depart from the parent ion before it is returned. According to the finding of Arbó *et al.* [22], in the bordering region between tunneling and over-the-barrier ionization, and in the over-the-barrier ionization regime, the average velocity of the ionized electrons is mainly determined by the Δp momentum transfer from the half-cycle of the laser pulse toward the electron. According to Eq. (5), with the

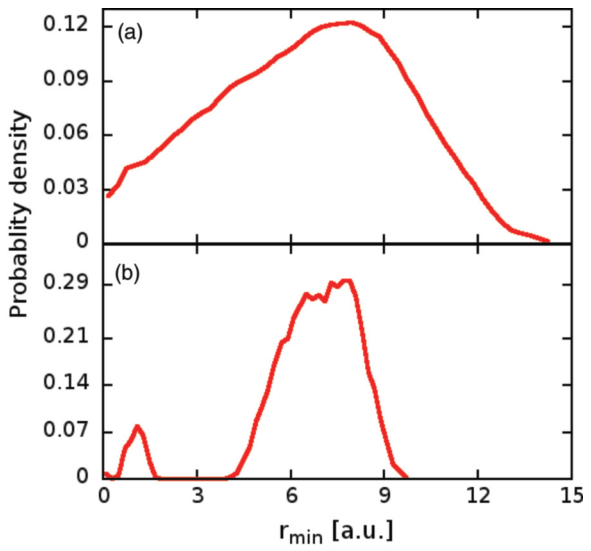

FIG. 9. (Color online) The distribution of the $r_{\min}$ values for (a) all scattered CTMC trajectories, and (b) scattered CTMC trajectories with $0.5 < p_{\text{per}} < 0.7$, and $0.7 < p_{\text{par}} < 0.9$. The distributions were normalized to 1.

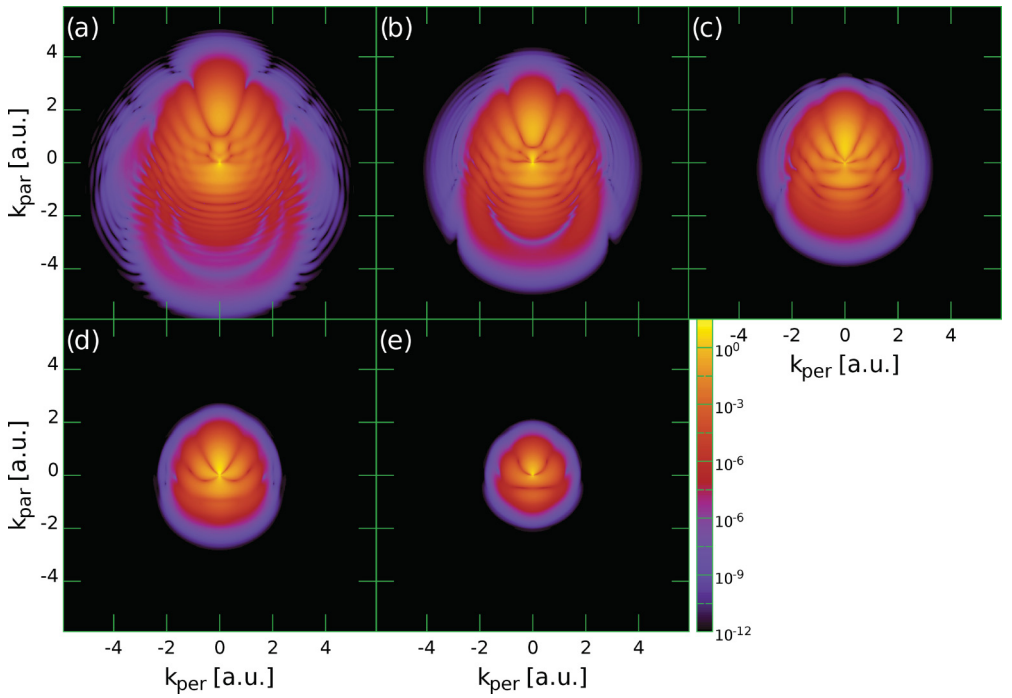

FIG. 10. (Color online) Ionization probability densities as a function of parallel and perpendicular momentum components at different field intensities, and at fixed $\omega = 0.4445$ a.u.; (a) $E_0 = 1$ a.u.; (b) $E_0 = 0.75$ a.u.; (c) $E_0 = 0.50$ a.u.; (d) $E_0 = 0.25$ a.u.; (e) $E_0 = 0.10$ a.u.

increase of z_0 the density of the HM interference fringes also increases.

In the remaining part of the present work, in the framework of the TDCC model, we will investigate how the value of z_0 influences the HM interference pattern. To achieve this, first we have fixed the laser field frequency at $\omega = 0.4445$ a.u. and we have decreased the field strength gradually from $E_0 = 1$ a.u. down to $E_0 = 0.1$ a.u. By doing so, we have decreased the average velocity of the wave packet, and implicitly of z_0. The momentum distribution of the free electrons obtained in the framework of the TDCC model for the chosen intensities is plotted in Fig. 10, where one can observe that by decreasing the field intensity (i.e., decreasing z_0), the density of the HM interference fringes also decreases.

Further, we have fixed the velocity of the electronic wave packet (by fixing the $\Delta p \sim E_0 T$ momentum transfer from a half-cycle of the laser field to the electron), and by increasing the period of the laser pulse we have increased the time interval available for the wave packet to propagate away from the core. This inherently increases the z_0 distance reached by the wave packet before its return. As we have observed previously, with increasing z_0, the density of the HM interference pattern also increased (see Fig. 11). This behavior is in good qualitative agreement with the prediction of the simple two-path model.

In addition to this qualitative comparison between the TDCC and the two-path models, we have also performed quantitative investigations. Since in our TDCC approach in each time moment we have access to the time-dependent wave function, we were able to follow in detail the electronic dynamics. For each set of laser pulse parameters, we have calculated the maximum distance reached by free electrons before their return. First, from the full wave function, we have subtracted the contribution of the bound states (i.e., negative energy eigenstates of the unperturbed $\hat{H}_0$ atomic Hamiltonian) using the Gram-Schmidt orthogonalization procedure, obtaining $\Psi_{\text{free}}(\vec{r},t)$. Then from $\Psi_{\text{free}}(\vec{r},t)$ we have calculated the expected value of $z(t)$:

$$z(t) = \frac{\langle \Psi_{\text{free}}(\vec{r},t)|\hat{z}|\Psi_{\text{free}}(\vec{r},t)\rangle}{\langle \Psi_{\text{free}}(\vec{r},t)|\Psi_{\text{free}}(\vec{r},t)\rangle}. \tag{12}$$

Since the quiver motion of the electrons is along the polarization of the laser field (along the Oz axis), from $z(t)$ the value of z_0 can be extracted directly. The z_0 values obtained for the laser pulse parameters used in the present work are presented in Table I. In most of the cases, these z_0 values are supporting the simple classical two-path picture [10] proposed for the interpretation of the HM's formation. However, the z_0 values corresponding to Figs. 10(d) and 10(e) are small,

TABLE I. The z_0 values obtained for different laser pulse parameters. The values are expressed in atomic units.

ω	τ	E_0	z_0
0.4445	28.26	1.0	8.13
0.4445	28.26	0.75	6.06
0.4445	28.26	0.50	4.02
0.4445	28.26	0.25	2.67
0.4445	28.26	0.10	1.47
0.666 75	18.84	0.5	5.74
0.4445	28.26	1.0	8.13
0.222 25	56.51	1.5	13.07

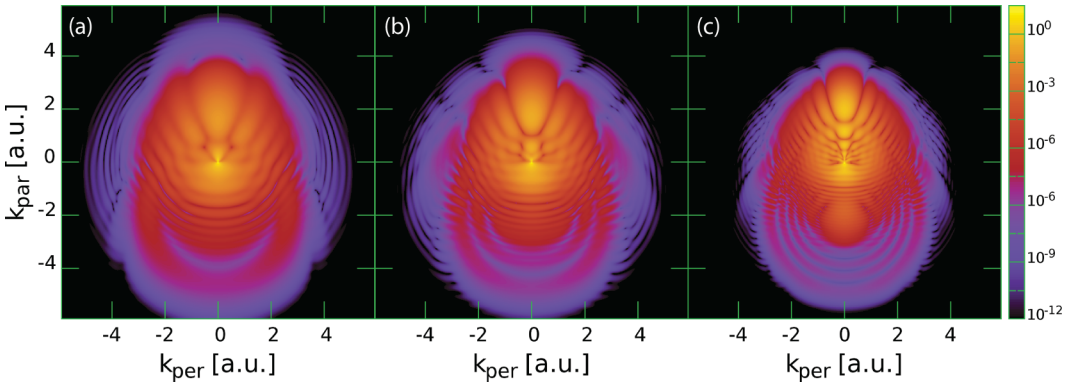

FIG. 11. (Color online) Ionization probability densities as a function of parallel and perpendicular momentum components at different field parameters: (a) $\omega = 0.666\,75$ a.u., $\tau = 18.84$ a.u., $E_0 = 1.5$ a.u.; (b) $\omega = 0.4445$ a.u., $\tau = 28.26$ a.u., $E_0 = 1$ a.u.; (c) $\omega = 0.222\,25$ a.u., $\tau = 56.51$ a.u., $E_0 = 0.50$ a.u.

indicating that the formed free electronic wave packets do not leave the immediate vicinity of the parent ion at low intensities. This points out the limits of the HM's classical interpretation, since at these intensities the formation of the spatially separated direct and scattered classical electron trajectories is no longer possible. In this case, the formation of the HM interference pattern can be interpreted as a result of a complex population exchange between the bound and free parts of the wave function during the rescattering, rather than as a result of interference between the direct and scattered electron trajectories.

For each z_0 value, we have calculated the two-path HM pattern using Eq. (5), and we have compared it with the TDCC HM patterns shown in Figs. 10 and 11. To make the comparison easier, in Fig. 12 we have plotted a cut from these HM patterns along a fixed $|\vec{p}|$ value for different laser pulse parameters. We have normalized both the TDCC (thick line) and the two-path (thin line) curves to their maximum value. In agreement with the previous deduction, in Fig. 12 we demonstrate that with decreasing z_0, the density of the HM also decreases in both models. We note, however, that significant discrepancies are also present. Considering any set of laser field parameters, the TDCC model, compared to the two-path model, predicts a much denser HM pattern. In addition to this, the TDCC and two-path HM pattern also differs in the relative height of the neighboring interference maxima: In the two-path model, all the interference maxima have the same height, while in the case of the TDCC model we have a central maximum at $\theta = 0$ followed by side maxima with decreasing height. These discrepancies are present due to the simplicity of the two-path model. In the two-path model, the distribution of the electrons in the source wave packet is considered to be uniform. This, together with the core considered as a uniform point scatterer, leads to the HM pattern, where each maximum has the same height. The denser TDCC HM pattern can be explained by the fact that in the two-path model, the phase accumulated by the electron on the scattered path is underestimated due to the neglect of the core's Coulomb potential. In the framework of the TDCC model, on the scattered path, the electron in the ingoing phase is accelerated, while in the outgoing phase it is decelerated to its initial velocity, leading to a larger average electron velocity and implicitly to a larger accumulated electron phase compared to the two-path model.

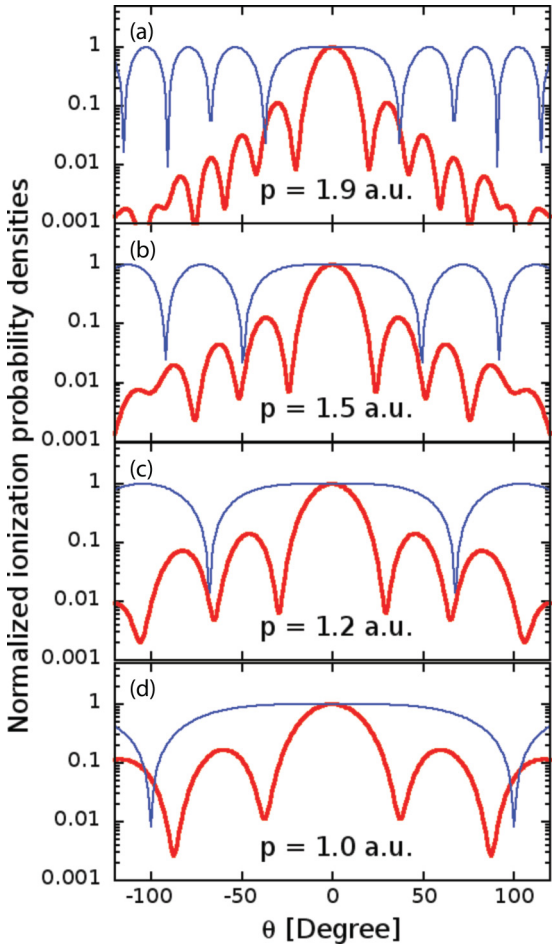

FIG. 12. (Color online) Ionization probability densities as function of electron ejection angle for fixed p electron momentum values and for different laser pulse parameters: $\omega = 0.4446$ a.u., $\tau = 28.26$ a.u. (a) $E_0 = 1.0$ a.u., (b) $E_0 = 0.75$ a.u., (c) $E_0 = 0.5$ a.u., (d) $E_0 = 0.25$ a.u. The thick line denotes the TDCC, while the thin line denotes the two-path model results. The θ electron ejection angle is measured from the laser polarization (i.e., Oz) axis.

IV. CONCLUSIONS AND OUTLOOK

In the present work, the ionization of the H atom induced by two-cycle XUV laser pulses in the tunneling and over-the-barrier regimes was studied. We have investigated in detail the time evolution of our system, and we have identified the dominant processes that were present. In addition to the different ionization mechanisms, we have identified the interference between electronic wave packets emitted at different time moments (temporal interference) and the interference between wave packets emitted at the same time, but following different paths (spatial interference). Since during the spatial interference the superposition of a direct (unperturbed) and a scattered (by the parent ion) wave occurs, the spatial interference can be considered as the HM of the target atom. Due to the fact that the HM can be an efficient tool to study the atomic structure, a significant part of our recent work was dedicated to studying the properties of the HM interference pattern in the XUV region using *ab initio* quantum-mechanical and classical calculations. Using CTMC simulation, we have confirmed the existence of two different types of interfering electron trajectories: the direct ones (far from the parent ion) and the scattered ones (close to the core). By performing TDCC calculations for different laser pulse parameters, in agreement with the simple two-path model of Huismans *et al.* [10], we have concluded that the shape of the HM interference pattern is mainly determined by the z_0 parameter, which measures how far the electronic wave packet departed from the parent ion before it was driven back by the laser field. We also found that for an optimal HM pattern, which is not too dense, and also not too sparse, we should have $z_0 = 10 \pm 5$ a.u. This paired with the other condition for the formation of the HM pattern, i.e., the existence of a closely packed electronic wave packet in the continuum (usually formed via tunneling or over-the-barrier ionization) fixes the laser pulse parameters as a function of ionization potential. For atoms with an ionization potential close to 0.5 a.u. for the experimental observation of the HM interference pattern, XUV laser pulses are required with a peak intensity of the order of 10^{15} W cm^{-2}. This is far from the experimentally available intensities, but with the further development of the pulse generation techniques, it may be available in the near future.

ACKNOWLEDGMENTS

This work was supported by the Sectoral Operational Programme for Human Resources Development 2007-2013, co-financed by the European Social Fund, under Projects No. POSDRU 89/1.5/S/60189 and No. POSDRU/107/1 5/S/76841, by a grant of the Romanian National Authority for Scientific Research, CNCS UEFISCDI Project No. PN-II-ID-PCE-2011-3-0192, and partially the Hungarian Scientific Research Fund OTKA No. NN 103279.

[1] A. Baltuska, T. Udem, M. Uiberacker, M. Hentschel, E. Goulielmakis, C. Gohle, R. Holzwarth, V. S. Yakovlev, A. Scrinzi, T. W. Hansch, and F. Krausz, Nature (London) **421**, 611 (2003).
[2] L. V. Keldysh, Sov. Phys. JETP **20**, 1307 (1965).
[3] X.-B. Bian, Y. Huismans, O. Smirnova, K.-J. Yuan, M. J. J. Vrakking, and A. D. Bandrauk, Phys. Rev. A **84**, 043420 (2011).
[4] F. Lindner, M. G. Schätzel, H. Walther, A. Baltuška, E. Goulielmakis, F. Krausz, D. B. Milošević, D. Bauer, W. Becker, and G. G. Paulus, Phys. Rev. Lett. **95**, 040401 (2005).
[5] D. G. Arbó, E. Persson, and J. Burgdörfer, Phys. Rev. A **74**, 063407 (2006).
[6] D. G. Arbó, K. L. Ishikawa, K. Schiessl, E. Persson, and J. Burgdörfer, Phys. Rev. A **81**, 021403 (2010).
[7] D. G. Arbó, K. L. Ishikawa, K. Schiessl, E. Persson, and J. Burgdörfer, Phys. Rev. A **82**, 043426 (2010).
[8] R. Gopal, K. Simeonidis, R. Moshammer, T. Ergler, M. Dürr, M. Kurka, K.-U. Kühnel, S. Tschuch, C.-D. Schröter, D. Bauer, J. Ullrich, A. Rudenko, O. Herrwerth, T. Uphues, M. Schultze, E. Goulielmakis, M. Uiberacker, M. Lezius, and M. F. Kling, Phys. Rev. Lett. **103**, 053001 (2009).
[9] T. Marchenko, Y. Huismans, K. J. Schafer, and M. J. J. Vrakking, Phys. Rev. A **84**, 053427 (2011).
[10] Y. Huismans, A. Rouzée, A. Gijsbertsen, J. H. Jungmann, A. S. Smolkowska, P. S. W. M. Logman, F. Lépine, S. Z. C. Cauchy, T. Marchenko, J. M. Bakker, G. Berden, B. Redlich, A. F. G. van der Meer, H. G. Muller, W. Vermin, K. J. Schafer, M. Spanner, M. Y. Ivanov, O. Smirnova, D. Bauer, S. V. Popruzhenko, and M. J. J. Vrakking, Science **331**, 61 (2011).
[11] M. Okunishi, T. Morishita, G. Prümper, K. Shimada, C. D. Lin, S. Watanabe, and K. Ueda, Phys. Rev. Lett. **100**, 143001 (2008).
[12] S. Micheau, Z. Chen, A. T. Le, J. Rauschenberger, M. F. Kling, and C. D. Lin, Phys. Rev. Lett. **102**, 073001 (2009).
[13] J. Xu, Z. Chen, A.-T. Le, and C. D. Lin, Phys. Rev. A **82**, 033403 (2010).
[14] C. D. Lin, A.-T. Le, Z. Chen, T. Morishita, and R. Lucchese, J. Phys. B **43**, 122001 (2010).
[15] C. I. Blaga, J. Xu, A. D. DiChiara, E. Sistrunk, K. Zhang, P. Agostini, T. A. Miller, L. F. DiMauro, and C. D. Lin, Nature (London) **483**, 194 (2012).
[16] J. Colgan and M. S. Pindzola, Phys. Rev. Lett. **88**, 173002 (2002).
[17] B. I. Schneider and L. A. Collins, J. Non-Cryst. Solids **351**, 1551 (2005).
[18] J. Feist, S. Nagele, R. Pazourek, E. Persson, B. I. Schneider, L. A. Collins, and J. Burgdörfer, Phys. Rev. A **77**, 043420 (2008).
[19] R. Abrines and I. C. Percival, Proc. Phys. Soc. London **88**, 861 (1966).
[20] R. E. Olson and A. Salop, Phys. Rev. A **16**, 531 (1977).
[21] K. Tökési and G. Hock, Nucl. Instrum. Methods Phys. Res., Sect. B **86**, 201 (1994).
[22] D. G. Arbo, M. S. Gravielle, K. I. Dimitriou, K. Tokesi, S. Borbely, and J. E. Miraglia, Eur. Phys. J. D **59**, 193 (2010).